HEAT AND MASS TRANSFER DURING PNEUMATIC CONVEYING DRYING OF LAMELLAR MATERIAL

A. WEISS, F. MAYINGER and E. RITTERSHAUS
Lehrstuhl A für Thermodynamik, Technische Universität München
Arcisstraße 21, 80333 München, Germany

Experiments on the pneumatic conveying drying of lamellar material showed that particle rotation exerts a strong influence on heat and mass transfer. High-speed photographs of these rotation processes supplied characteristic initial figures for a theoretical analysis, which works with mean time values of the projection areas. The calculation process presented here corresponds well with the experiment and is tailored to use in practice.

1. INTRODUCTION

The investigation into heat and mass transfer during pneumatic conveying drying of lamellar material was carried out using cut tobacco stems, a sub-product of industrial cigarette production.

The bulk particles of this material are pourable and are similar to rolled oats in contour and size.

For existing flat, thin particles characterizations of disperse two-phase systems for non-spherical particles which are known so far meet only relatively limited demands for accuracy as regards transport behaviour during pneumatic conveying against gravity and thus the drying process. The aim of the work was therefore to develop better suited product and process descriptions and process related measuring techniques required for the experimental check.

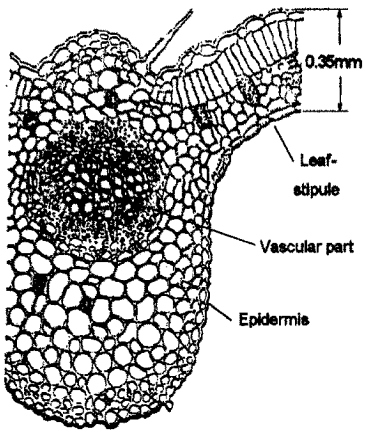

Fig. 1: Cross section of the central part of the midstem of a tobacco leaf [1]

2. PRODUCT

From the structure and anatomy of the tobacco leaf (Fig. 1) some important stem and cut stem characteristics can be derived regarding form and drying behaviour.

The cross section of the midstem of a tobacco shows near the leaf stipule a vascular part; this is a tubular system which supplies the living plant with nutrients from the roots. Around this vascular area there are cellular structures which have a supporting function, embedded in the epidermis, a sort of derma, which protects the tobacco e.g. from drying out.

Due to the structure described it is clear that internal water transfer resistance lengthways along the stem can be assumed to be very slight; this makes plausible the assumption of constant drying rates as from certain moistures and particle sizes.

The leaf lamina is separated from the fermented stalks by threshing before leaving the producer country. This separation process produces rodlike fragments which are 30 to 100 mm long and 2.5 to approx. 8 mm thick. After moistening to 40 % water content, the leaf stems are fed to a special cutter in such a way that the cuts preferably run diagonally to the longitudinal axis. The cut widths selected are 0.12; 0.2 and 0.25 mm. Thus thin, flat, almost even particles are produced, the contours of which are circular or rectangular. They are then dried to the final product moisture level by pneumatic conveying drying.

To characterize the particles and the particle distribution 4 fractions of certain classes are first

established by sieving, and these are sorted manually into circular or rectangular disks. The particles which are thus spread out, as shown in Fig. 2 for the sieve fraction of smaller 3.15 mm and larger 2.0 mm mesh width, are photographed and evaluated as to their average projection area using digital image processing.

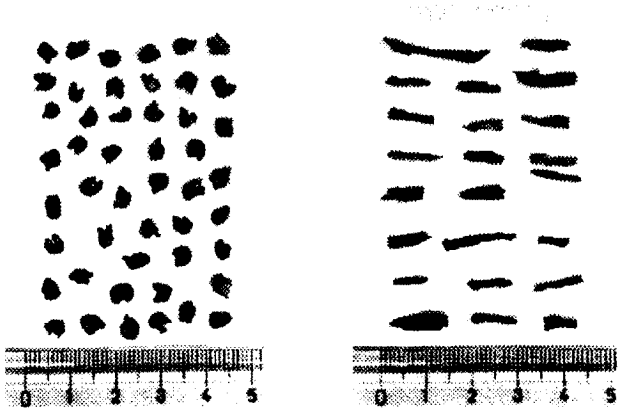

Average circle diameter 3,5 mm

Average rectangle dimensions 10,4 mm x 1,7 mm

Fig 2: Cut stems of sieve fraction 3.15 mm > x > 2 mm, sorted into "circles" and "rectangles". (Cut width: 0,2 mm)

With this information and the most frequent edge ratio of the rectangular particles and the cut width and density which is constant to all particles it is possible to calculate characteristic values per mass fraction. This example produces a circular disk diameter of 3.5 mm and rectangular dimensions of 10.4 x 1.7 mm. The two largest sieve fractions can be combined in view of their similar measurements, so the method produces 6 fractions, in each case 3 basic forms of circles and rectangles. The behaviour of the particles during pneumatic transport is dealt with in Section 5 und 7.

3. PILOT PLANT

The pilot plant is a single-stage pneumatic conveying dryer on a pilot scale (Fig. 3).

In 5 positions, at different levels in the dryer, there are measuring planes for analyzing air temperatures, humidity and particle velocity. The material is fed either unilaterally or mirror symmetrically via metering tubes, weight conveyors, vibrating conveyors and cellular wheel sluices with chutes into the narrowest cross section of the drying tower.

To separate the material from the air a cyclone separator is scheduled. The material is fed out through two cellular wheel sluices in sequence. The volume of drying air is measured with an orifice and regulated

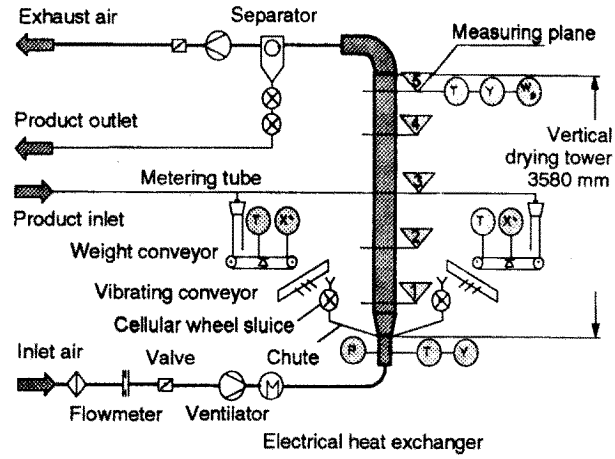

Fig. 3: Diagram of pilot plant

with a throttle valve and via the ventilator rotational speed. An electrical heat exchanger heats the air.

The almost rectangular cross section of the drying tower is equipped on the measuring planes with 4 connection pieces, facing each other in pairs, in which the sensors are placed. Display windows permit visual observation of the particle flow.

To determine the relative particle overflow the empty tube flow profile of the air can be taken as a reliable basis for the scheduled loading of the air with material.

For reducing local differences in air temperatures and humidity over the cross section of the drying duct the mirror symmetrical material input proved to be by far the most effective solution. With a more even dispersion of material the measurement differences were halved.

To validate the model preference was therefore given to bilateral input and the remaining differences taken into account by taking the suitable means. In addition, only stationary operating conditions were evaluated.

4. MEASURING TECHNIQUES

4.1 Measuring temperature

The best method proved to be the installation of a resistance thermometer directly in the drying duct,as shown in Fig. 4.

High-speed video photographs show that, given the prescribed solid material loading of the flow, contacts between the cut stems and the thermometer only occur sporadically. In particular, the measuring point is not touched because of rejuvenation in the flow direction.

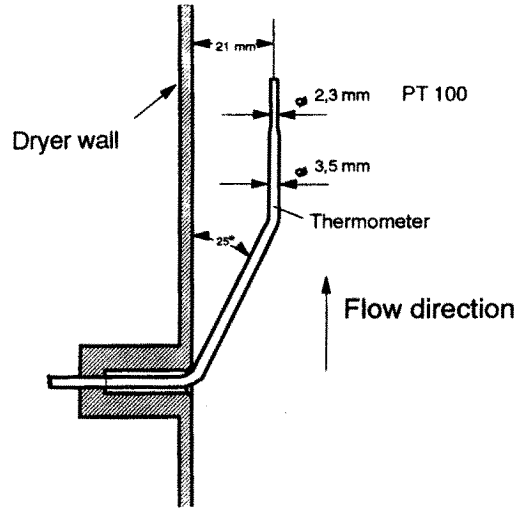

Fig. 4: Measuring temperature in the drying duct

4.2. Measuring humidity

Every measuring plane had to be analysed simultaneously with relatively great accuracy so as to obtain corresponding humidities at all levels of the measuring duct in spite of unavoidable brief fluctuations in the process.

With separate measuring devices per plane, depending on the measuring principle, this is either too inaccurate or very expensive. For this reason a storage system was developed which permits the simultaneous removal of air samples on each measuring plane and behind the cyclone separator and its storage so that the humidity of the stored drying air samples can be measured in series with the same infrared spectrometer.

Presumed errors due to the adulteration of samples in the store could not be found; for one reason because only half the contents of each store of 3 litres were evaluated after 3.3 times the store volume of drying gas has flown through.

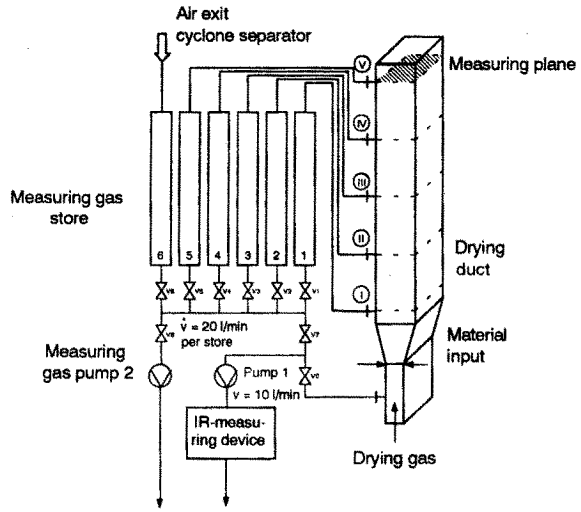

Fig. 5: Storage system for drying air samples

4.3. Particle velocity

Mean particle velocity was measured via semi-automatic evaluation of high-speed video photographs with the aid of digital image processing. Picture frequency is 6.000 per second (Fig. 6).

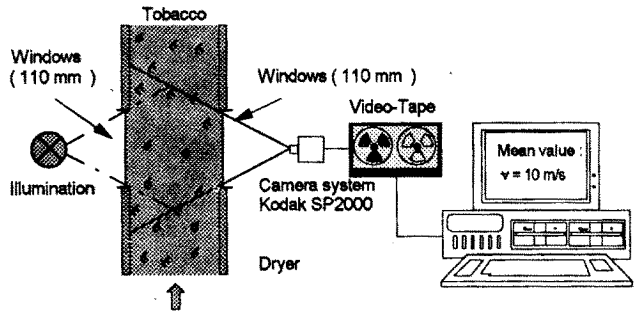

Fig. 6: Measurement system to determine particle velocity

As the overall depth of the flow cross section was analysed, the image perspective had to be compensated for.

The video system screen shows three similar images superimposed at intervals of 1/6.000 second. Using digital picture processing and Fourier analysis a binary image is made from each triple image and the path covered per 1/6.000 second by the corresponding particle triples (Fig. 7).

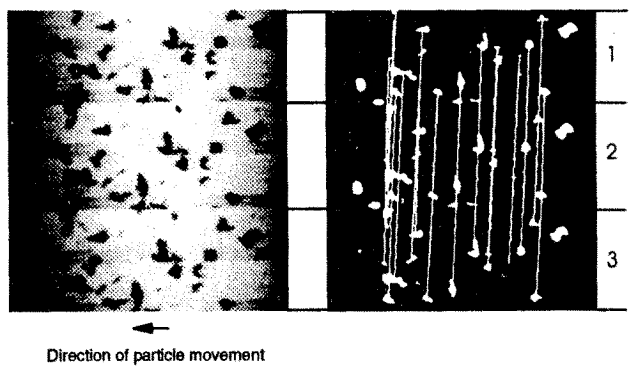

Fig. 7: Triple image of the video system and corresponding binary image

The process works with a measurement inaccuracy of only ± 1.5 %.
The image evaluation method used is based on solutions followed by Chávez [2] to analyse the spray behaviour of nozzles used to disperse liquids.

5. MATHEMATICAL MODEL OF PNEUMATIC CONVEYING DRYING

5.1. Projection areas and characteristic particle lengths, drag coefficient

The evaluation of the high-speed videos also shows that one-dimensional particle velocity is superposed by particle rotation of between 3 and 25 Hz. It is therefore advisable to use the mean time value of the projection areas of the rotating flat circular and rectangular discs to calculate drag. This can be easily determined for very thin discs if uniform rotation is assumed. The projection of the main measurement D which is undergoing sinus vibration can then be time averaged without taking account of the thickness.
The equation for the mean time projection area of a rotating rectangular disc for L, B. > S is thus

$$\underline{AP} = \frac{2}{\pi} LB \qquad (1)$$

Analogous for a circular disc (D > S)

$$\underline{AP} = \frac{1}{2} D^2 \qquad (2)$$

The characteristic length of the rotating individual particles are also easy to describe with the definition provided by Krischer [3] and the above-mentioned marginal conditions. To calculate the characteristic length as the ratio of particle surface to circumference of effective projection area the average time figure of this circumference has proved its value. For rectangular discs, however, it must be remembered that they prefer to rotate around their longitudinal axis.
This characteristic length of a uniformly rotating circular disc is

$$d_{pl} = 0,603\, D \qquad (3)$$

for rectangular dics (rotating around the transverse axis)

$$d_{pl,R1} = \frac{BL}{\frac{2}{\pi}L + B} \qquad (4)$$

for rectangular discs (rotation around the longitudinal)

$$d_{pl,R2} = \frac{BL}{L + \frac{2}{\pi}B} \qquad (5)$$

The weighting of the time shares of the flight position of the rectangles is made via the relative times $t_{R1,r} = 0,2$ und $t_{R2,r} = 0,8$.

$$d_{pl} = t_{R1,r}\, d_{pl,R1} + t_{R2,r}\, d_{pl,R2} \qquad (6)$$

The drag coefficient can be described independent of positon [4], [5].

$$C_W = \frac{24}{Re} + \frac{5,5}{\sqrt{Re}} + 1,1 \qquad (7)$$

5.2 Differential equation system

With the aid of Eq. (8) to (12) and some other algebraic equations and statements on the transfer and physical properties the following system of linked differential equations provides satisfactory solutions.
Changes in particle velocity

$$\frac{dw_{pl}}{dl} = \frac{1}{w_{pl} M_{pl}} \left[F_{Wl} + F_{Al} + F_{Gl} + F_{RWl} \right] \qquad (8)$$

Changes in particle moisture

$$\frac{dX_i}{dl} = \frac{1}{w_{pl} M_{p0l}} \dot{M}_{pDl} \qquad (9)$$

Changes in particle temperature

$$\frac{d\vartheta_{pl}}{dl} = \frac{1}{w_{pl} M_{p0l} c_{ppl}} \qquad (10)$$

$$x \left\{ \dot{Q}_{pol} + \dot{M}_{pDl} \left[\vartheta_{pl} \left(c_{pW} \Big|_0^{\vartheta_{pl}} - c_{pD} \Big|_0^{\vartheta_{pl}} \right) - h_{VD}(0°C) \right] \right\}$$

Changes in the humidity of the drying air

$$\frac{dY}{dl} = \mu \sum_{i=1}^{n} \frac{m_i}{w_{pl} M_{p0l}} \dot{M}_{pDl} \qquad (11)$$

Changes in the temperature of the drying air

$$\frac{d\vartheta_f}{dl} = \mu \frac{1}{c_{pf0} + c_{pD} Y} \left\{ \frac{1}{\dot{M}_{p0}} Uk(\vartheta_u - \vartheta_f) + \right. \quad (12)$$

$$\left. \sum_{i=1}^{n} \frac{m_i}{w_{pi} M_{p0i}} \left[\dot{M}_{pDi} \left(c_{pD} \Big|_0^{\vartheta_p} \vartheta_p - c_{pD} \Big|_0^{\vartheta_p} \vartheta_f \right) - \dot{Q}_{p\alpha i} \right] \right\}$$

Particle collisions need not be taken into account because of the low loading but there are wall contacts which reduce the mean particle velocity the length of the dryer. This is accounted for by introducing wall friction F_{RWi} [6].

For this problem calculating the heat and mass transfer figures is possible with the empirical Nußelt number which was taken over by Krischer and Kast [3], based on taking the means of the functions gained from parallelly flowed plates of the Reynolds und Prandtl number for laminar and turbulent flow conditions in the boundary layer Eq. (13), (14), (15).

$$Nu_i = \frac{\alpha_i d_{pi}}{\lambda_{fm}} = \sqrt{Nu_{lam,i}^2 + Nu_{turb,i}^2} \quad (13)$$

$$Nu_{lam,i} = 0{,}664\, Re_i^{0,5} Pr^{0,33} \quad (14)$$

$$Nu_{turb,i} = \frac{0{,}037\, Re_i^{0,81} Pr}{1 + 2{,}443\, Re_i^{-0,1} (Pr^{0,67} - 1)} \quad (15)$$

The masss transfer coefficient is determined with the aid of the Lewis number, analogous to heat transfer, Eq. (16).

$$\frac{\beta_i}{\alpha_i} = \frac{1}{c_{pfm} \rho_{fm} Le_m^{2/3}} \quad (16)$$

6. TEST PROGRAMME

To check the model 5 tests were carried out:

① the parameter variations of the loading of the air with material,
given a constant air flow,

② given a constant material flow,

③ the variation of cut stem width,

④ u. ⑤ the variation in air temperatures in two parties of material of different average stem diameter

7. COMPARISON BETWEEN EXPERIMENT AND CALCULATION

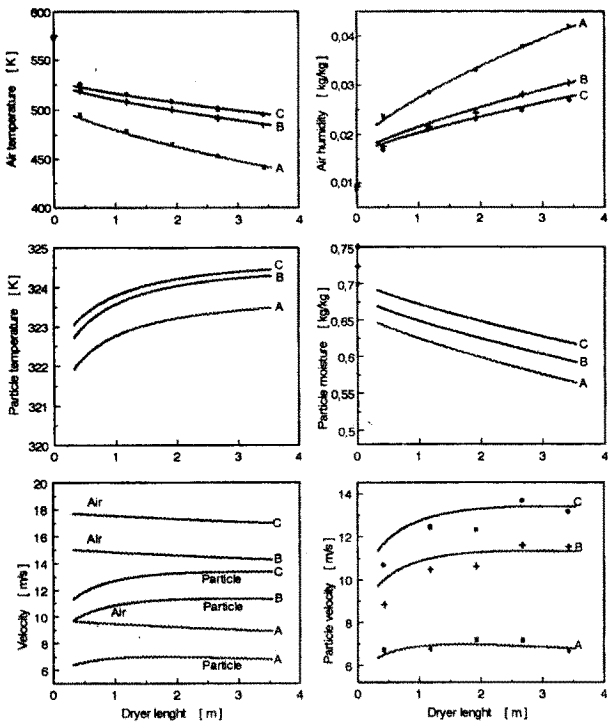

Fig. 8: Test series ② A, B, C: Loading the air with material $\mu_A = 0{,}2461$, $\mu_B = 0{,}1629$, $\mu_C = 0{,}1372$

As the model has no adaptation parameters other than a particle-wall friction constant, it is all the more important for a comparison between the values measured and the mathematical forecasts for the whole test programme to coincide very well and without exception.

To represent the five test series the coincidence achieved is briefly discussed by taking the example of test series ② A, B, C, i.e. the loading variation of the air with material given a constant material flow and otherwise comparable initial parameters.

The 6 graphs (Fig. 8) show the most important figures which characterize the drying process over the whole length of the dryer, such as air temperatures and humidity, particle temperatures and moisture, and air and particle velocity. The key to success is in the correct forecasting of the particle velocities measured. As can be seen, the figures vary by max. ± 0,5 m/s around the calculated velocity curve.

As the loading of the air with mass was reduced by increasing the flow of the body of air, air velocity and thus particle velocity is highest for C. The relative velocity which for C is clearly higher than for A, shows

the connection between particle-wall friction and absolute particle velocity.

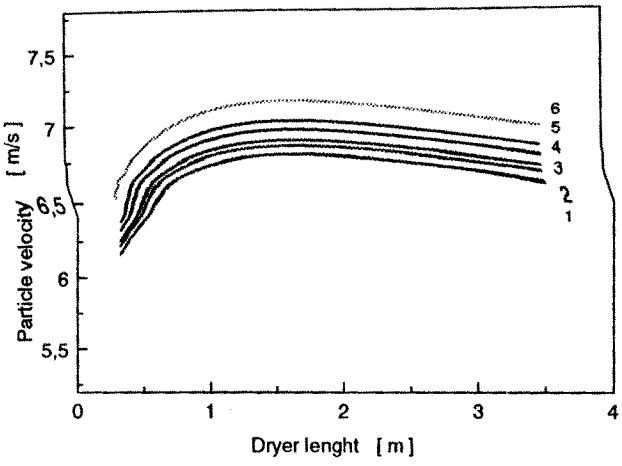

Fig. 9: Test Nr. ② A: Loading the air with material = 0,2461. Calculated particle velocities, classified according to mass fractions 1 to 6

The relative velocity, which for C is only slightly higher than for B as a result of the relatively slight differences in loading, means that the decreases in air temperature and thus the increases in humidity hardly differ over the whole length. A differs noticeably from this. Here the higher residence time due to lower air and particle velocity is dominant and in spite of lower driving forces achieves material moisture comparable to that of B and C. As can be seen, the particle moistures are almost identical, taking account of their initial moistness.

The particle temperatures are also on a similar level. With the latter calculations the model quantifies particle characteristics which practically cannot be measured directly within the drying duct.

A fractional analysis of particle velocities shows a phenomenon typical of cut stems, i.e. that large and small cut stems fly through the dryer on average with only 0.5 m/s difference (Fig.9).

This is due to the constant ratio of particle volume to effective projection area. - In the case of spherical particles, however, the third dimension leads to far more variable velocities between large and small particles.

NOMENCLATURE

AP	projektion area
B	width
C_w	drag coefficient
c_p	heat capicity
D	diameter
d	characteristic length
F_A	lift force
F_G	gravity force
F_{RW}	wall friction force
F_W	drag force
h_{VD}	evaporation enthalpie of water
k	thermal transmittance
L	length
Le	Lewis number
l	coordinate of dryer height
M	mass
$\dot{M}$	mass flow
m	part by mass
Nu	Nußelt number
Pr	Prandtl number
Q	heat flow
S	thickness
t	time
U	circumference
w	velocity
X	material moisture
Y	air humidity (dry basis)

Greek formulae

α	heat-transfer coefficient
β	mass-transfer coefficient
ϑ	temperature
λ	thermal conductivity
μ	mass loading of air

Indices, symbols

α	convective heat transfer
D	steam
f	air, fluid
i	fraction counter
m	mean value
n	number of fractions
p	particle
R1	rectangular disc, rotating round transverse axis
R2	rectangular disc rotating round longitudinal axis
r	relative
W	water, drag, wall
Symbols*	total system, balance room
0	dry. dry weight

REFERENCES

[1] **Melchior, H.**, 1970, Handbuch der Lebensmitteltechnik, 6. Band, pp. 414-425, Springer Verlag Berlin Heidelberg New York

[2] **Chávez, A.**, 1991, Holographische Untersuchung an Einspritzstrahlen, Fluiddynamik und Wärmeübergang durch Kondensation, Dissertation, TU München

[3] **Krischer, O., Kast, W.**, 1978, Die wissenschaftlichen Grundlagen der Trocknungstechnik, 3. Auflage, Band 1, pp. 132-134, Springer Verlag Berlin Heidelberg New York

[4] **Brauer, H.**, 1971, Grundlagen der Einphasen- und Mehrphasenströmungen, pp. 211-213, Verlag Sauerländer, Aarau und Frankfurt am Main

[5] **Christiansen, E.B., Barker, D.E.**, 1965, The Effect of Shape and Density on the Free Settling of Particles at High Reynolds Numbers, A.J.Ch.E. Journal, Vol. 11, No. 1, pp. 145-151

[6] **Kemp, J.C., Oakley, D.E., Bahu, R.E.**, 1991, Computational Fluid Dynamics, Modelling Of Vertical Pneumatic Conveying Dryers, Powder Technology, No. 65, pp. 477-484